

# An ecologically-based approach to terrestrial primary production

Grayson Badgley<sup>1,2,+,\*</sup>, Leander D.L. Anderegg<sup>1,3,+</sup>, Joseph A. Berry<sup>1</sup>, Christopher B. Field<sup>2,4</sup>

1. Department of Global Ecology, Carnegie Institution for Science, Stanford, CA, 94305

2. Department of Earth System Science, Stanford University, Stanford, CA, 94305

3. Department of Integrative Biology, University of California, Berkeley, CA, 94720

4. Woods Institute for the Environment, Stanford University, Stanford, CA, 94305

\* badgley@stanford.edu

+ These authors contributed equally

## 1 Abstract

2 Terrestrial gross primary production (GPP) is both the largest and most uncertain flux within the  
3 global carbon cycle. Much of this uncertainty results from the fact that GPP is onerous to measure  
4 and is only reliably monitored at roughly 100 canopy-scale sites scattered across the globe. Sparsity  
5 of consistent observations of GPP at the site-level translates into significant uncertainties in our  
6 understanding of the magnitude and spatial distribution of GPP at the global scale. We present a  
7 new, ecologically-based approach for estimating terrestrial photosynthesis that combines high  
8 accuracy in reproducing site-based GPP estimates, yet allows for simple calculation using data  
9 available globally for more than three decades. Our approach takes advantage of the tendency for  
10 plants to only capture the amount of sunlight they are capable of efficiently using. By precisely  
11 measuring the investment plants dedicate toward light capture, we estimate global annual terrestrial  
12 photosynthesis to be 147 Pg C y<sup>-1</sup> (95% credible interval 131-163 Pg C y<sup>-1</sup>), which exceeds  
13 prevailing, machine learning based GPP estimates by over 20%. Furthermore, our approach allows  
14 for the propagation and exploration of multiple sources of uncertainty in our estimation of GPP,  
15 allowing for biological, statistical, and retrieval errors to be separately examined.

## 16 Introduction

17 Terrestrial photosynthesis (or gross primary production (GPP)) is responsible for fixing anywhere  
18 from 119 to 169 Pg C  $y^{-1}$ , making GPP both the largest and most uncertain component of the global  
19 carbon cycle [1]. Carbon fixed by photosynthesis in turn provides the basis for practically all life on  
20 land, providing a strong motivation for improving global estimates of GPP. It is especially important  
21 to understand how GPP might respond to global environmental change, as minor perturbations in  
22 terrestrial productivity have implications for global biodiversity, agriculture, and climate change [2,  
23 3].

24 Quantifying terrestrial GPP is a complicated task, requiring precise measurements of the  
25 exchange of both energy and CO<sub>2</sub> between the land surface and the atmosphere. In these efforts,  
26 eddy covariance measurements of land surface CO<sub>2</sub> exchange have proved an invaluable asset for  
27 estimating canopy and ecosystem scale photosynthesis and subsequent model validation [4, 5].  
28 Despite their utility, eddy covariance measurements are limited in both time and space; individual  
29 flux sites measure CO<sub>2</sub> fluxes over approximately 1 km<sup>2</sup> and, in any given year, fewer than 100 sites  
30 operate globally [6]. Such limitations especially hinder the validation of terrestrial ecosystem models,  
31 which operate globally at resolutions much greater than a single kilometer and over time periods  
32 ranging from years to decades.

33 As a result, a host of semi-empirical upscaling approaches have emerged for translating site-level  
34 CO<sub>2</sub> fluxes to globally gridded photosynthesis estimates suitable for model benchmarking and  
35 development. Though many upscaling schemes exist, two approaches are by far the most widely  
36 applied: machine learning [7, 8] and remote sensing [9]. Both approaches leverage *in situ* fluxes to  
37 construct models relating site-level abiotic characteristics, plant traits, and meteorology to estimate  
38 photosynthesis beyond tower footprints. Upscaling allows for both the investigation of the drivers of  
39 global photosynthesis [10, 11] and for more extensive benchmarking of photosynthesis models by  
40 expanding the temporal and spatial availability of photosynthesis estimates [12, 13].

41 Yet any upscaling introduces uncertainties into GPP estimates, stemming both from model  
42 formulation and model inputs. Machine learning approaches, for example, provide the best possible  
43 constraint on GPP based on available data, but they functionally operate as black boxes. As a  
44 result, they make it difficult to diagnose causes and consequences of uncertainty, limiting their utility  
45 for permanently improving our process-based understanding of photosynthesis. Further limitations  
46 are introduced by the availability of and the uncertainties contained within input datasets (e.g.

47 meteorological data) used for upscaling.

48 Here, we report a novel approach for estimating global GPP that avoids many of these  
49 limitations. The approach uses the near-infrared reflectance of vegetation ( $\text{NIR}_V$ ), a  
50 reflectance-based index that is highly correlated with measured site-level GPP [14]. This correlation  
51 is a consequence of  $\text{NIR}_V$  integrating information on both canopy light capture and time-averaged  
52 light-use efficiency, which does not have a unique spectral signal, but is instead expressed through  
53 canopy structure. Plants endeavor to only capture light they are capable of using; any strategy  
54 capturing more or less light would be inefficient and subject to the pressures of natural selection [15].  
55 This optimality criterion, termed the resource balance or co-ordination hypothesis, means any  
56 measure of investment in light capture can serve as the basis for estimating GPP [16, 17].  
57 Investment in light capture provides an index of canopy potential photosynthetic capacity, which  
58 should in turn closely match total resource availability. This approach has a long history in  
59 estimating net primary production (NPP) or biomass production, beginning with Monteith [18], who  
60 showed that a number of agricultural crops all converted sunlight into dry matter at a rate of  
61 approximately  $1.4 \text{ g MJ}^{-1}$ . This approach was extended to utilize satellite-based measures of light  
62 capture and applied to the global scale [19, 20]. But limitations in the available satellite indices  
63 meant that accurate estimates required additional information on temperature and moisture levels.  
64 Because  $\text{NIR}_V$  integrates both light capture and light-use efficiency, it provides a uniquely useful  
65 index of investment in light capture and should be sufficient for estimating GPP without additional  
66 information on meteorological conditions. This avoids limitations in data availability and makes our  
67 approach capable of estimating GPP at high spatial resolution.

68 We present our results in three parts. First, we validate the  $\text{NIR}_V$ -GPP relationship at the site  
69 and global scale. Second, we extend the relationship to consider global GPP. Third, we evaluate  
70 some limitations in the global dataset of  $\text{NIR}_V$  and in the consistency of the  $\text{NIR}_V$ -GPP relationship.

## 71 Results

72 Using Bayesian hierarchical modeling, we found that  $\text{NIR}_V$ , combined with information on leaf habit  
73 (deciduous, evergreen, and crop) explained 68% of the variation in annual GPP at 105  $\text{CO}_2$   
74 monitoring sites (526 site-years that passed quality-control and data completeness requirements) and  
75 had an RMSE of  $0.36 \text{ kg C m}^{-2} \text{ y}^{-1}$  (Fig. 1, see Methods). The approach required no additional  
76 information on meteorological conditions, such as site temperature or incoming radiation, indicating

77 that  $\text{NIR}_V$  captures the effects of meteorology on GPP and supporting our interpretation of  $\text{NIR}_V$  as  
 78 an integrator of whole-plant resource optimization (Fig. S1). Fewer inputs not only reduces  
 79 uncertainty from input datasets, but also allows the  $\text{NIR}_V$  approach to be applied across a wide  
 80 range of spatial and temporal scales. By contrast, existing remote sensing and machine learning  
 81 based approaches for estimating GPP often require tens to hundreds of inputs. The  $\text{NIR}_V$  approach  
 82 performed similarly well at the monthly time scale (Fig. 1, inset), explaining 56% of the observed  
 83 variation in monthly GPP with an RMSE of  $0.08 \text{ kg C m}^{-2} \text{ mo}^{-1}$ . The RMSE of  $\text{NIR}_V$ -based  
 84 estimates of annual GPP was 42% lower than the RMSE of GPP fluxes calculated from BESS, a  
 85 physiologically-based land surface model. Annual RMSE was 57% higher than GPP estimates from  
 86 FLUXCOM, a meteorological-based, statistical upscaling of FLUXNET GPP fluxes (Table S1).

87 For annual GPP, the most parsimonious model included just three leaf habits, with a single  
 88 intercept and separate  $\text{NIR}_V$ -GPP slopes for sites with i) evergreen, ii) deciduous, and iii) crop leaf  
 89 habits, as well as increasing variance in both residual error and site-level random intercepts as a  
 90 function of  $\text{NIR}_V$  (Fig. S2). Further dividing leaf habits into biomes resulted in minor model  
 91 improvements, but an almost identical Deviance Information Criteria with more parameters, causing  
 92 us to adopt the simpler three leaf habit model (see Methods).

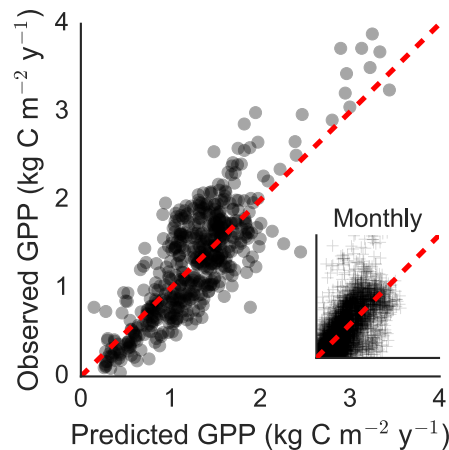


**Figure 1.  $\text{NIR}_V$  explains a large portion of site-level GPP at both the A) monthly and B) annual timescale.** Note the relatively large variation in monthly GPP estimates for low values of observed GPP, as compared to the near-zero intercept in the case of annual fluxes.

93 Applying this site-level scaling to globally resolved measurements of  $\text{NIR}_V$ , we estimated the  
 94 median value of global annual GPP to be  $147 \text{ Pg C y}^{-1}$ , with a 95% credible interval of  $131\text{-}163 \text{ Pg C}$   
 95  $\text{y}^{-1}$ . Our median GPP estimate was intermediate between estimates from spatial models and  
 96 constraints from  $\text{O}_2$  isotopes. FLUXCOM places annual GPP at  $118 \text{ Pg C y}^{-1}$ , while BESS puts

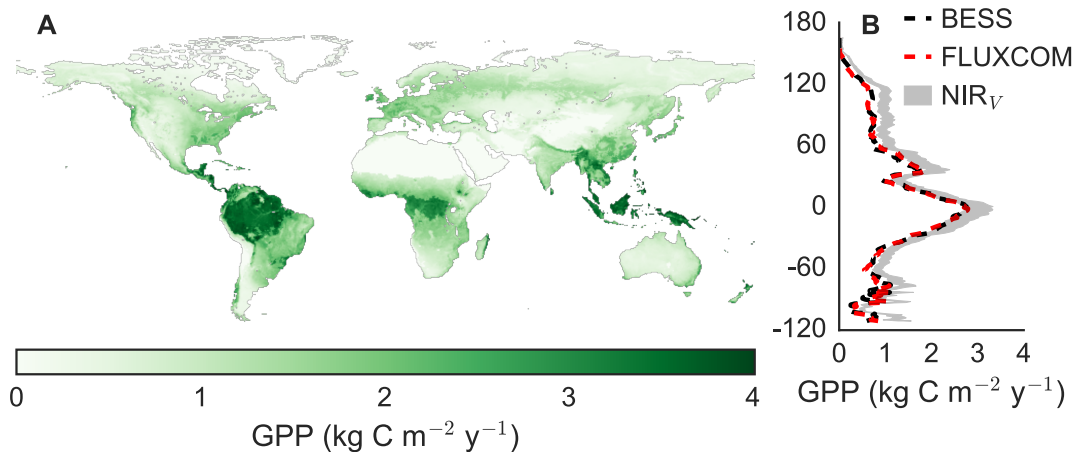


**Figure 2.** The A) global and B) latitudinal distribution of NIR<sub>v</sub>-derived GPP. Mapped estimates represent the median value of 1000 semi-independent upscalings of NIR<sub>v</sub>, while the full 95% credible range of GPP is shaded in grey for latitudinal estimates. The latitudinal distribution of average total annual GPP as estimated by FLUXCOM and BESS are shown for comparison.

97 mean global GPP at 122 Pg C y<sup>-1</sup>. A meta-analysis of model-based annual GPP estimates ranged  
 98 from 119 to 169 Pg C y<sup>-1</sup> [1]. By contrast, O<sub>2</sub> isotopic measurements are consistent with global  
 99 annual GPP in the range of 150 to 175 Pg C y<sup>-1</sup> [21].

100 The spatial distribution of NIR<sub>v</sub>-derived GPP was consistent with existing global GPP estimates,  
 101 further validating our approach (Fig. 2). As expected, GPP was concentrated in the tropics and  
 102 declined toward the poles. On a per biome basis, tropical forests contributed the most to global  
 103 GPP, accounting for 31% of global GPP; FLUXCOM and BESS attribute 34% and 33% of GPP to  
 104 tropical forests, respectively. Though lower in relative terms, NIR<sub>v</sub>-derived GPP in tropical forests  
 105 was 15% higher than both FLUXCOM and BESS GPP estimates in absolute terms. Instead, NIR<sub>v</sub>  
 106 assigned higher productivity to the midlatitudes, especially midlatitude mixed forests, grassland, and  
 107 shrub-dominated ecosystems (Fig. 2B; Table S2). One recent data assimilation study that combined  
 108 solar-induced chlorophyll fluorescence with a terrestrial ecosystem model found similar relative  
 109 increases in extratropical GPP [22].

110 When compared on a per pixel basis, NIR<sub>v</sub> was strongly linear with both FLUXCOM and BESS  
 111 at the annual time scale, with R<sup>2</sup> exceeding 0.90 for both products and per pixel RMSE below 0.4 kg  
 112 C m<sup>-2</sup> y<sup>-1</sup>, further emphasizing the robustness of NIR<sub>v</sub>-derived GPP estimates (Fig. 3). This  
 113 consistency is striking, given that our approach employed only two variables (NIR<sub>v</sub> and leaf habit),  
 114 while both FLUXCOM and BESS require numerous environmental inputs. The comparison also

115 emphasizes that NIR<sub>V</sub>-derived GPP estimates were consistently higher than existing approaches,  
 116 exceeding FLUXCOM GPP by a median value of 0.24 kg C m<sup>-2</sup> y<sup>-1</sup> and BESS GPP by 0.21 kg C  
 117 m<sup>-2</sup> y<sup>-1</sup>. There are several possible reasons for this difference. On the one hand, NIR<sub>V</sub> might  
 118 represent a theoretical upper bound of photosynthesis, prior to consideration of physiological effects  
 119 (e.g., water or nutrient limitation), causing NIR<sub>V</sub>-based GPP estimates to outpace  
 120 physiologically-based approaches. Alternatively, both BESS and FLUXCOM might systematically  
 121 underestimate true GPP. Investigating the source of this discrepancy through more detailed  
 122 comparisons of NIR<sub>V</sub> against eddy covariance data and site-level modelling represents an important  
 123 next step in using NIR<sub>V</sub> to study photosynthesis at the global scale.

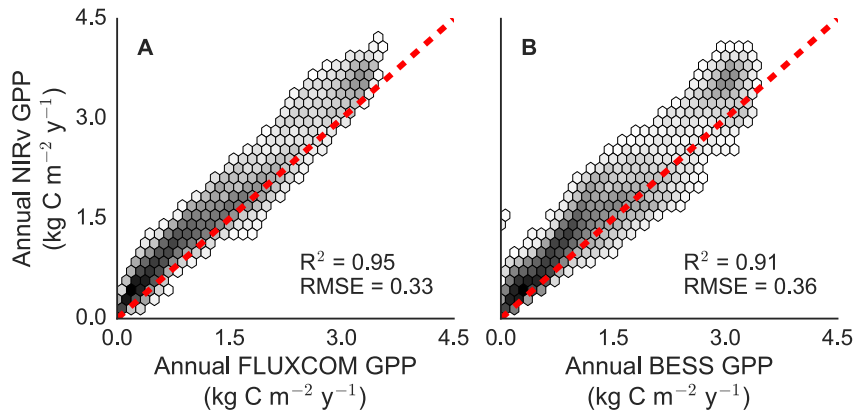


**Figure 3. Upscaled NIR<sub>V</sub>-based estimates of annual GPP are linear with both A) FLUXCOM and B) BESS GPP estimates.** NIR<sub>V</sub>-based estimates exhibit a slight positive bias relative to both FLUXCOM and BESS, though low overall RMSE. NIR<sub>V</sub>-based GPP estimate shown as the median case of 1000 semi-independent upscalings, see Methods.

124 Model parsimony, combined with Bayesian estimation, allowed us to propagate three sources of  
 125 uncertainty on a per pixel basis: statistical, variation in per leaf habit scaling; site, deviation of a  
 126 site intercept from the global per-leaf-habit relationship; and residual, or otherwise unexplained  
 127 errors. Median per pixel uncertainty was 0.20 kg C m<sup>-2</sup> y<sup>-1</sup> and total uncertainty, comprising all  
 128 three sources of error, peaked in the tropics where total annual NIR<sub>V</sub> was highest. In the worst case,  
 129 the 95% credible interval of GPP exceeded as much as 0.75 kg C m<sup>-2</sup> y<sup>-1</sup> in the Amazon basin and  
 130 Indonesia (Fig. 4A). Given that tropical forests constitute the highest proportion of GPP (exceeding  
 131 30%), high uncertainty throughout the tropics significantly contributes to the overall uncertainty of  
 132 global GPP estimates, regardless of approach.

133 Informative patterns emerge from examining the relative importance of statistical, site, and  
 134 residual uncertainty on a per pixel basis; two examples of pixel-level uncertainties are shown in Fig.

135 4B. Outside of pixels with especially low  $\text{NIR}_V$ , statistical uncertainty was always lowest, indicating  
 136 minimal uncertainty in per leaf habit scaling. On average, site uncertainty was always largest,  
 137 meaning there was more uncertainty in the  $\text{NIR}_V$ -GPP relationship from site to site than existed  
 138 year to year (encompassed by residual uncertainty) at a single site. This indicates that either  $\text{NIR}_V$   
 139 or GPP estimates are not comparable across sites, which can only be addressed by improving the  
 140 accuracy of both measurements. The predominance of site-level uncertainty is a direct result of  
 141 considerable variation in the site-level intercept found in our initial upscaling (Fig. 1). Site-to-site  
 142 variability is randomly distributed, showing no relationship with site climate, thus highlighting  
 143 retrieval errors (e.g., soil reflectance, clouds, mismatches between tower and remote sensing  
 144 footprints) as the likely cause of site-level uncertainty (Fig. S2).

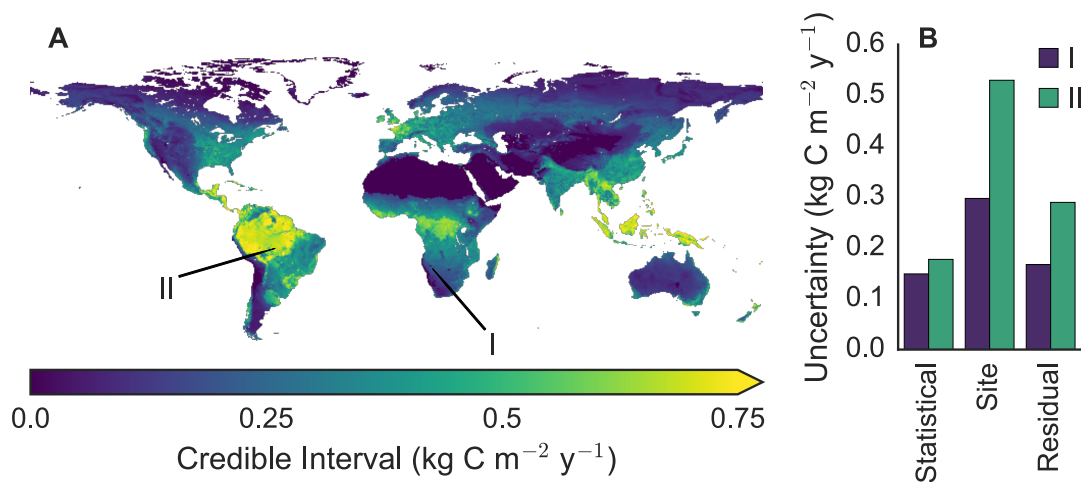


**Figure 4. Bayesian hierarchical modeling allows for per pixel error estimation.** A) Uncertainty in GPP peaks in the tropics (especially the Amazon and Indonesia), where the credible range of GPP can range by over  $0.75 \text{ kg C m}^{-2} \text{y}^{-1}$ . B) On a per pixel basis, site-level uncertainty is typically largest.

## 145 Discussion

146  $\text{NIR}_V$  takes advantage of a globally consistent relationship between canopy structure and  
 147 photosynthetic potential to provide an ecologically-grounded approach for estimating GPP that  
 148 combines a very simple formulation with excellent performance at validation sites (Figs. 1 and 3).  
 149 As a result,  $\text{NIR}_V$  provides a novel means for upscaling GPP flux measurements that is largely  
 150 independent of existing and widely used semi-empirical and process-based approaches. Finally, the  
 151  $\text{NIR}_V$ -based GPP approach achieves strong statistical performance while maintaining parsimony,

152 allowing for i) an evolutionary and ecologically mechanistic interpretation of upscaling results, ii)  
153 easy introspection of uncertainty and how uncertainty is partitioned between model structure and  
154 inputs (Fig. 4) and iii) simple calculation.

155 Parsimony allows for a mechanistic interpretation of the NIR<sub>V</sub>-GPP relationship, in terms of how  
156 NIR<sub>V</sub> and GPP jointly relate to canopy architecture and light capture. From a physical standpoint,  
157 NIR<sub>V</sub> relates to variations in canopy leaf area and leaf display, serving as a useful index of the  
158 investment plants dedicate toward light capture [14]. Consistent with the resource balance  
159 hypothesis, plants tend to capture only as much light as they are capable of using [16], helping  
160 explain the strength of the NIR<sub>V</sub>-GPP relationship that otherwise has no strong physiological basis  
161 (Fig. 1). On an instantaneous basis, environmental factors like water, light, and temperature  
162 combine with leaf-level biochemical capacity to dictate the rate of photosynthesis; insights that are  
163 enshrined in leaf-level photosynthesis models [23]. The predictive ability of NIR<sub>V</sub>, without the need  
164 for additional inputs like total incoming radiation, indicates that canopy architecture, as opposed to  
165 physiology alone, controls photosynthetic fluxes at longer time scales.

166 This mechanistic interpretation of the NIR<sub>V</sub>-GPP relationship has implications for terrestrial  
167 photosynthesis models. We postulate that neglecting changes in canopy architecture within models  
168 can cause decoupling of light capture and canopy physiology. Models typically hold canopy  
169 architectural parameters (e.g., the ratio of sun and shade leaves) constant and instead vary leaf  
170 physiological parameters, like the maximum rate of carboxylation ( $V_{C_{max}}$ ). During periods of peak  
171 growth, for example, a model might underestimate light capture and compensate by arbitrarily  
172 adjusting  $V_{C_{max}}$  to match GPP observations. This can result in  $V_{C_{max}}$  becoming a  
173 model-dependent parameter, as opposed to a biologically interpretable measurement [12]. Future  
174 studies should consider combining measurements of NIR<sub>V</sub> and  $V_{C_{max}}$  to address this problem.  
175 These data would allow for independently fixing model  $V_{C_{max}}$  using empirical data, while  
176 simultaneously varying canopy architecture as a function of observed NIR<sub>V</sub>. Such an experiment  
177 would capitalize on the empirical NIR<sub>V</sub>-GPP relationship to improve how process-based models  
178 represent both light capture and leaf physiology.

179 The NIR<sub>V</sub> approach also allows for statistically valid error propagation (Fig. 4). More  
180 complicated approaches to estimating GPP make it difficult to accurately partition sources of error,  
181 especially model structural errors and errors due to input uncertainties. Minimizing upscaling  
182 complexity largely eliminates this problem. In particular, we were surprised by the predominance of  
183 site-level error; the NIR<sub>V</sub>-GPP relationship always varied more from site to site than within a single

184 site (Fig. 4B). This indicates that either the biology controlling the NIR<sub>V</sub>-GPP relationship itself  
185 varies from site to site or that NIR<sub>V</sub> and GPP measurements lack consistency across space. More  
186 simply, if the NIR<sub>V</sub>-GPP relationship holds in general, deviations from this relationship should have  
187 either a biological or a methodological interpretation. The simplicity of our approach allows for the  
188 investigation of both possibilities.

189 As an example of measurement challenges, we noticed a stark disagreement in the NIR<sub>V</sub>-GPP  
190 relationship at an eddy covariance site in French Guyana, GF-GUY. GPP fluxes at GF-Guy varied  
191 less than 20% month to month, while NIR<sub>V</sub> varied by a factor of three (Fig. 5A). Assuming accurate  
192 GPP estimates, the divergence suggests errors in NIR<sub>V</sub> observations at the site. We suspected cloud  
193 contamination, as remote sensing in the tropics is notoriously plagued by clouds degrading the  
194 accuracy of satellite measurements. To investigate this, we used the newly available MAIAC data  
195 product, which uses atmospheric modelling to remove aerosols, sub-pixel clouds, and other artifacts  
196 from MODIS satellite imagery [24]. The variability of NIR<sub>V</sub> dramatically reduced with the MAIAC  
197 data (Fig. 5A). In fact, MAIAC-derived NIR<sub>V</sub> had a smaller dynamic range than observed GPP,  
198 strongly indicating cloud contamination of the baseline MODIS dataset both at GF-Guy and, in all  
199 likelihood, throughout the tropics. Such contamination would reduce our median global GPP  
200 estimate, making 147 Pg C y<sup>-1</sup> a conservative estimate of global GPP. Using MAIAC-derived NIR<sub>V</sub>  
201 as the basis for estimating GPP would reduce site-level uncertainty and improve the accuracy of  
202 global GPP estimates. Unfortunately, such efforts will have to wait for a globally consistent MAIAC  
203 reprocessing of the full MODIS record.

204 Fundamental differences in plant physiology that govern the NIR<sub>V</sub> and GPP relationship can also  
205 explain the predominance of site uncertainty. In this case, the simplicity of our approach leaves out  
206 potentially important biological determinants of productivity. Take for example the difference in C3  
207 and C4 photosynthesis. C4 plants fix CO<sub>2</sub> more efficiently than C3 plants, which should cause a  
208 steeper slope in the NIR<sub>V</sub>-GPP relationship, all else equal. When we examined a trio of Nebraskan  
209 eddy covariance towers that annually rotate between soy (C3) and corn (C4) crops, we found  
210 significant differences in the NIR<sub>V</sub>-GPP slope with crop type (Fig. 5B). As with cloud  
211 contamination, including information on the distribution of C3 and C4 vegetation across both wild  
212 and managed ecosystems would likely increase our global estimate of GPP, as C3 sites comprise the  
213 majority of data within the dataset used for calibration and further emphasizing the conservative  
214 nature of our 147 Pg C y<sup>-1</sup> estimate of GPP. Apart from indicating that NIR<sub>V</sub>-based GPP estimates  
215 could be further improved by incorporating a photosynthetic pathway parameter, this result

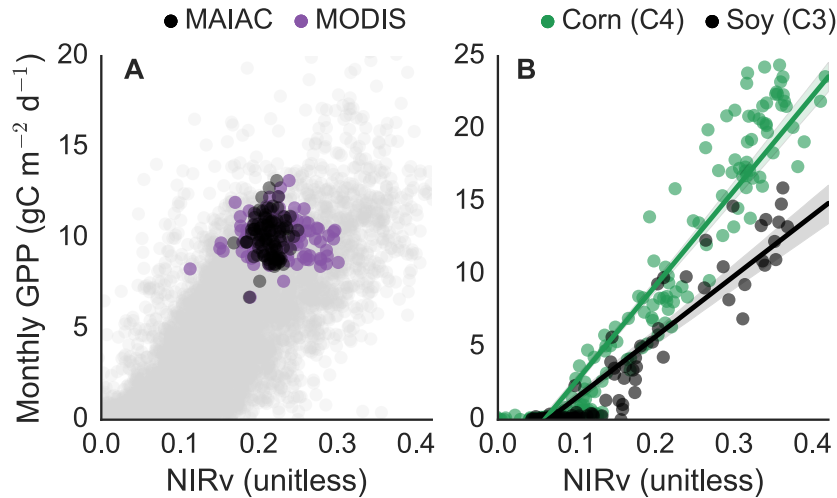


**Figure 5. Parsimony allows for the investigation of sources of model uncertainty.** A) Cloud contamination drives large monthly variations in MODIS collection 6  $\text{NIR}_V$  that are not matched by variations in  $\text{NIR}_V$ . All monthly data from the FLUXNET2015 dataset shown in grey. B) Photosynthetic pathway predictably alters the  $\text{NIR}_V$ -GPP relationship, as C4 plants have measurably higher light use efficiencies.

216 demonstrates how our ecologically-grounded approach can be used to study plant physiology at the  
 217 global scale.

218 The third and final advantage of the  $\text{NIR}_V$  approach is that  $\text{NIR}_V$  can be calculated from existing  
 219 high-resolution and widely available satellite imagery. This makes  $\text{NIR}_V$  immediately available for  
 220 benchmarking models at spatial and temporal scales relevant to land surface models, whether the  
 221 model runs at 30 meters for a specific study site or spans the globe (Figs. 1 and 3). Our approach for  
 222 estimating GPP from  $\text{NIR}_V$  could also be calculated for the full Landsat and MODIS records, as well  
 223 as the entire 39 year record of the Advanced Very High Resolution Radiometer (AVHRR) series of  
 224 sensors [25]. Long-term records that cover a range of climatic conditions are vital for benchmarking  
 225 physiological models we hope to use in forecasting future ecological change. Finally, the ease of  
 226 measuring  $\text{NIR}_V$  allows researchers to make relatively cheap, canopy-scale spectral measurements  
 227 that are directly comparable against satellite data, facilitating efforts to bridge spatial scales.

228 To conclude, we have developed a new, largely independent approach for estimating GPP based  
 229 on principles of evolutionary optimality and that closely corresponds to existing best-in-class GPP  
 230 estimates. Our robust handling of uncertainty demonstrates that current estimates of global GPP are  
 231 likely too low and that the annual productivity of terrestrial ecosystems likely exceeds  $147 \text{ Pg C y}^{-1}$ .  
 232 Further refinement of our  $\text{NIR}_V$ -based approach, through reducing input uncertainty and inclusion  
 233 of additional physiological processes, will serve as a powerful new tool for validating terrestrial

234 ecosystem models and improving our mechanistic understanding of the terrestrial carbon cycle.

## 235 **Materials and Methods**

### 236 **Data**

237 We compared  $\text{NIR}_V$  against monthly and annual GPP fluxes at 105 flux sites contained in the  
238 FLUXNET2015 Tier 1 dataset. For each site, we downloaded 500 meter, daily red (620-670nm) and  
239 near-infrared (NIR, 841-876nm) nadir bidirectional reflectance distribution function adjusted  
240 reflectance data from MODIS collection MCD43A4.006 hosted on Google Earth Engine [26]. We  
241 calculated median NDVI and NIR for all daily MODIS pixels overlapping a  $1\text{km}^2$  circle centered on  
242 the location of each fluxsite. All gaps were filled using linear interpolation. Finally, we multiplied  
243 median NDVI by NIR to calculate  $\text{NIR}_V$  and took the average of all daily  $\text{NIR}_V$  values for each  
244 month. We then combined monthly  $\text{NIR}_V$  estimates with monthly observations of GPP from the  
245 FLUXNET2015 dataset (variable name: GPP\_VUT\_MEAN). We required all site-months to have  
246 over 75% valid GPP observations and required site-years to have a minimum of 9 months of data.  
247 We gridded the MCD43A4.006 dataset to  $0.5^\circ$  to serve as the basis of our global upscaling.

248 In addition to the site-level comparisons, we evaluated  $\text{NIR}_V$ -based GPP estimates against two  
249 existing models of GPP: FLUXCOM, a machine learning approach for upscaling FLUXNET  
250 observations [8], and GPP estimates derived from the physiologically-based land surface model, the  
251 Breathing Earth System Simulator (BESS), which has been extensively benchmarked against eddy  
252 covariance measurements of GPP [27, 28]. We used the mean ensemble of annual GPP<sub>HB</sub> fluxes  
253 from the FLUXCOM CRUNCEPv6 product, accessed via the FLUXCOM website. For BESS, we  
254 used GPP estimates from BESS V1, obtained from the BESS website. Site-level RMSE values for  
255 FLUXCOM and BESS were derived from data provided by the authors [8, 28].

### 256 **Calibration**

257 We used Bayesian estimation to relate  $\text{NIR}_V$  and leaf habit to GPP at both monthly and annual  
258 timescales. Bayesian estimation allows the propagation of uncertainty through hierarchical modeling,  
259 which allowed us to fit slope and intercept terms, as well as hierarchical variance terms capturing  
260 site-level random effects (random deviations from the global slope and intercept per site) and error  
261 variance [29]. We specified GPP as a linear function of  $\text{NIR}_V$ , with the best model (according to the

262 Deviance Information Criteria; [29]) consisting of a single, near-zero intercept and differing slopes for  
263 evergreen, deciduous, and crop leaf habits. The model included two additional terms: a random  
264 site-level intercept term and an error term that were both normally distributed with mean of 0 and  
265 variance exponentially related to multi-year average  $\text{NIR}_V$ . See Supplementary Text 1 and Table S3  
266 for a full description of the model structure, as well as alternative model structures tested.

267 We used Markov chain Monte Carlo simulations (MCMC) implemented in JAGS [30] to sample  
268 the joint posterior distribution of fitted models, with initial diffuse priors for all parameters. We ran  
269 three parallel MCMC chains, evaluated chains for convergence, and thinned chains to remove  
270 within-chain autocorrelation, producing 1000 nearly independent draws from the posterior. We  
271 calculated site-level, median estimates of GPP and 95% credible intervals for model parameters  
272 based on the joint posterior distribution of the best model. We have posted the GPP calibration  
273 code to [www.github.com/badgley/nirv-global](http://www.github.com/badgley/nirv-global).

## 274 **Upscaling**

275 We produced global annual estimates of GPP with the best annual  $\text{NIR}_V$  model, using all 1000  
276 draws from the joint model posterior to calculate GPP for all land pixels from 2005 to 2015. For  
277 each posterior draw, we calculated GPP of every pixel based on the per-biome scaling parameter  
278 plus randomly sampled site-level and residual error based on the site and residual variance  
279 parameter estimates for that draw. Using the site-level model for our global upscaling captures  
280 correlations between parameter estimates (scaling slope and site-level variance estimates were often  
281 correlated), resulting in GPP estimates that appropriately represent statistical, site, and residual  
282 uncertainty from the full joint posterior distribution of the model. We present the median and 95%  
283 credible intervals from the distribution of the upscaled GPP estimates. Pixels with the landcover  
284 classification “barren” were excluded from the analysis.

## 285 **Acknowledgments**

We thank Jennifer Johnson and Yoichi Shiga for the many conversations that clarified our thinking,  
as well as Youngryel Ryu and Mary Whelan, whom reviewed earlier drafts of this work. Gianluca  
Tramontana and Chongya Jiang kindly provided site-level GPP fluxes for comparison. Bin Peng  
shared the C3/C4 crop rotation data. Funds from a NASA Earth and Space Science fellowship (GB),  
a NOAA Climate and Global Change fellowship (LDLA), and NSF Postdoctoral Research Fellowship

Grant No. DBI-1711243 (LDLA) supported this research. Any opinions, findings, and conclusions or recommendations expressed in this material are those of the author(s) and do not necessarily reflect the views of the National Science Foundation. This work used eddy covariance data acquired and shared by the FLUXNET community, including these networks: AmeriFlux, AfriFlux, AsiaFlux, CarboAfrica, CarboEuropeIP, CarboItaly, CarboMont, ChinaFlux, Fluxnet-Canada, GreenGrass, ICOS, KoFlux, LBA, NECC, OzFlux-TERN, TCOS-Siberia, and USCCC. The ERA-Interim reanalysis data are provided by ECMWF and processed by LSCE. The FLUXNET eddy covariance data processing and harmonization was carried out by the European Fluxes Database Cluster, AmeriFlux Management Project, and Fluxdata project of FLUXNET, with the support of CDIAC and ICOS Ecosystem Thematic Center, and the OzFlux, ChinaFlux and AsiaFlux offices.

## References

- [1] A. Anav, P. Friedlingstein, C. Beer, P. Ciais, A. Harper, C. Jones, G. Murray-Tortarolo, D. Papale, N. C. Parazoo, P. Peylin, et al. “Spatiotemporal patterns of terrestrial gross primary production: A review”. *Reviews of Geophysics* 53.3 (2015), pp. 785–818.
- [2] J. Rockström, W. Steffen, K. Noone, Å. Persson, F. S. Chapin III, E. F. Lambin, T. M. Lenton, M. Scheffer, C. Folke, H. J. Schellnhuber, et al. “A safe operating space for humanity”. *Nature* 461.7263 (2009), pp. 472–475.
- [3] S. W. Running. “A measurable planetary boundary for the biosphere”. *Science* 337.6101 (2012), pp. 1458–1459.
- [4] D. Baldocchi, E. Falge, L. Gu, R. Olson, D. Hollinger, S. Running, P. Anthoni, C. Bernhofer, K. Davis, R. Evans, et al. “FLUXNET: A new tool to study the temporal and spatial variability of ecosystem-scale carbon dioxide, water vapor, and energy flux densities”. *Bulletin of the American Meteorological Society* 82.11 (2001), pp. 2415–2434.
- [5] D. Baldocchi. “‘Breathing’ of the terrestrial biosphere: lessons learned from a global network of carbon dioxide flux measurement systems”. *Australian Journal of Botany* 56.1 (2008), pp. 1–26.
- [6] J. Kumar, F. M. Hoffman, W. W. Hargrove, and N. Collier. “Understanding the representativeness of FLUXNET for upscaling carbon flux from eddy covariance measurements”. *Earth System Science Data Discussions* (Aug. 2016).

- [7] C. Beer, M. Reichstein, E. Tomelleri, P. Ciais, M. Jung, N. Carvalhais, C. Rödenbeck, M. A. Arain, D. Baldocchi, G. B. Bonan, et al. “Terrestrial gross carbon dioxide uptake: global distribution and covariation with climate”. *Science* (2010), p. 1184984.
- [8] G. Tramontana, M. Jung, C. R. Schwalm, K. Ichii, G. Camps-Valls, B. Ráduly, M. Reichstein, M. A. Arain, A. Cescatti, G. Kiely, et al. “Predicting carbon dioxide and energy fluxes across global FLUXNET sites with regression algorithms”. *Biogeosciences* (2016).
- [9] S. W. Running, R. R. Nemani, F. A. Heinsch, M. Zhao, M. Reeves, and H. Hashimoto. “A continuous satellite-derived measure of global terrestrial primary production”. *BioScience* 54.6 (2004), pp. 547–560.
- [10] M. Jung, M. Reichstein, C. R. Schwalm, C. Huntingford, S. Sitch, A. Ahlström, A. Arneth, G. Camps-Valls, P. Ciais, P. Friedlingstein, et al. “Compensatory water effects link yearly global land CO<sub>2</sub> sink changes to temperature”. *Nature* 541.7638 (2017), pp. 516–520.
- [11] M. Zhao and S. W. Running. “Drought-induced reduction in global terrestrial net primary production from 2000 through 2009”. *Science* 329.5994 (2010), pp. 940–943.
- [12] G. B. Bonan, P. J. Lawrence, K. W. Oleson, S. Levis, M. Jung, M. Reichstein, D. M. Lawrence, and S. C. Swenson. “Improving canopy processes in the Community Land Model version 4 (CLM4) using global flux fields empirically inferred from FLUXNET data”. *Journal of Geophysical Research: Biogeosciences* 116.G2 (2011).
- [13] M. Williams, A. Richardson, M. Reichstein, P. Stoy, P. Peylin, H. Verbeeck, N. Carvalhais, M. Jung, D. Hollinger, J. Kattge, et al. “Improving land surface models with FLUXNET data”. *Biogeosciences* 6.7 (2009), pp. 1341–1359.
- [14] G. Badgley, C. B. Field, and J. A. Berry. “Canopy near-infrared reflectance and terrestrial photosynthesis.” *Science Advances* 3.3 (2017), e1602244.
- [15] A. J. Bloom, F. S. Chapin, and H. A. Mooney. “Resource limitation in plants - an economic analogy”. *Annual Review of Ecology and Systematics* 16 (1985), pp. 363–392.
- [16] C. B. Field. “Ecological scaling of carbon gain to stress and resource”. In: *Response of Plants to Multiple Stresses*. Academic Press San Diego, 1991, pp. 35–65.
- [17] V. Maire, P. Martre, J. Kattge, F. Gastal, G. Esser, S. Fontaine, and J.-F. Soussana. “The coordination of leaf photosynthesis links C and N fluxes in C<sub>3</sub> plant species”. *PloS One* 7.6 (2012), e38345.

- [18] J. L. Monteith. “Climate and the efficiency of crop production in Britain”. *Philosophical Transactions of the Royal Society London B* 281.980 (1977), pp. 277–294.
- [19] C. S. Potter, J. T. Randerson, C. B. Field, P. A. Matson, P. M. Vitousek, H. A. Mooney, and S. A. Klooster. “Terrestrial ecosystem production: a process model based on global satellite and surface data”. *Global Biogeochemical Cycles* 7.4 (1993), pp. 811–841.
- [20] C. B. Field, J. T. Randerson, and C. M. Malmström. “Global net primary production: combining ecology and remote sensing”. *Remote sensing of Environment* 51.1 (1995), pp. 74–88.
- [21] L. R. Welp, R. F. Keeling, H. A. Meijer, A. F. Bollenbacher, S. C. Piper, K. Yoshimura, R. J. Francey, C. E. Allison, and M. Wahlen. “Interannual variability in the oxygen isotopes of atmospheric CO<sub>2</sub> driven by El Niño”. *Nature* 477.7366 (2011), pp. 579–582.
- [22] A. J. Norton, P. J. Rayner, E. N. Koffi, M. Scholze, J. D. Silver, and Y.-P. Wang. “Estimating global gross primary productivity using chlorophyll fluorescence and a data assimilation system with the BETHY-SCOPE model”. *Biogeosciences Discussions* 2018 (2018), pp. 1–40.
- [23] G. D. Farquhar, S. von Caemmerer, and J. A. Berry. “A biochemical model of photosynthetic CO<sub>2</sub> assimilation in leaves of C<sub>3</sub> species”. *Planta* 149.1 (1980), pp. 78–90.
- [24] A. Lyapustin, J. Martonchik, Y. Wang, I. Laszlo, and S. Korkin. “Multiangle implementation of atmospheric correction (MAIAC): 1. Radiative transfer basis and look-up tables”. *Journal of Geophysical Research: Atmospheres* 116.D3 (2011).
- [25] M. E. Brown, J. E. Pinzón, K. Didan, J. T. Morisette, and C. J. Tucker. “Evaluation of the consistency of long-term NDVI time series derived from AVHRR, SPOT-vegetation, SeaWiFS, MODIS, and Landsat ETM+ sensors”. *IEEE Transactions on Geoscience and Remote Sensing* 44.7 (2006), pp. 1787–1793.
- [26] C. Schaaf and Z. Wang. “MCD43A4 MODIS/Terra+ Aqua BRDF/Albedo Nadir BRDF Adjusted RefDaily L3 Global 500 m V006”. *NASA EOSDIS Land Processes DAAC* (2015).
- [27] Y. Ryu, D. D. Baldocchi, H. Kobayashi, C. van Ingen, J. Li, T. A. Black, J. Beringer, E. Van Gorsel, A. Knohl, B. E. Law, et al. “Integration of MODIS land and atmosphere products with a coupled-process model to estimate gross primary productivity and evapotranspiration from 1 km to global scales”. *Global Biogeochemical Cycles* 25.4 (2011).

- [28] C. Jiang and Y. Ryu. “Multi-scale evaluation of global gross primary productivity and evapotranspiration products derived from Breathing Earth System Simulator (BESS)”. *Remote Sensing of Environment* 186 (2016), pp. 528–547.
- [29] A. Gelman, J. B. Carlin, H. S. Stern, and D. B. Rubin. *Bayesian data analysis*. Chapman and Hall/CRC, 1995.
- [30] M. Plummer. *JAGS: A program for analysis of Bayesian graphical models using Gibbs sampling*. 2003.

1 **Supplementary Information for**

2 **NIRv-GPP Supplement**

3 **Grayson Badgley, Leander D.L. Anderegg, Joseph A. Berry, Christopher B. Field**

4 **Grayson Badgley**

5 **E-mail: [badgley@stanford.edu](mailto:badgley@stanford.edu)**

6 **This PDF file includes:**

7     Supplementary text

8     Figs. S1 to S2

9     Tables S1 to S4

10    References for SI reference citations

## 11 **Supporting Information Text**

### 12 **Supplementary Text 1: Bayesian Modeling**

13 We used Bayesian estimation to fit linear mixed effects models relating GPP to  $\text{NIR}_V$ . For the sake of simplicity, we modeled  
14 annual or monthly GPP as a linear function of  $\text{NIR}_V$ , and explored a variety of model structures allowing both slopes and  
15 intercepts to differ by land cover class or leaf habit, with random site-level effects. Preliminary model selection suggested that  
16 site-level random slope and intercept terms were not needed for the annual model, but were needed for monthly model. For the  
17 annual model, we explored a variety of fixed effects structures, as well as a number of variance functions (for residual variation  
18 and site-level intercepts). See Table S3 for list of annual models explored and their associated Deviance Information Criteria  
19 scores (DIC). All error functions assumed normally distributed errors and similar functional forms for residual error and site  
20 random intercepts, but with residual errors being a function of observed annual  $\text{NIR}_V$  and site random intercepts a function of  
21 site mean annual  $\text{NIR}_V$ , treating true  $\text{NIR}_V$  as a latent variable) are easily implemented in this modeling framework, though  
22 we present the simplest defensible case for the sake of illustration and intuitive upscaling. We produced global annual estimates  
23 of GPP using the posterior distribution of the best annual  $\text{NIR}_V$  model (bolded in Table S3).

### 24 **Open Source Software**

25 **Python.** All analyses, with the exception of the Bayesian modeling, were performed using the Python programming language.  
26 We processed netCDF files and tabular data using xarray (1), pandas (2), and numpy (3). We used matplotlib (4) and seaborn  
27 (5) for visualization, and Jupyter notebooks for organizing analyses (6).

28 **R.** We ran all Bayesian modeling in the R programming environment (7), making use of the “r2jags” package (8) to interface  
29 with JAGS, a Bayesian modeling software package (9).

GPP Product	RMSE (kg C m <sup>-2</sup> y <sup>-1</sup> )
NIR <sub>v</sub>	0.36
BESS	0.55
FLUXCOM	0.20

**Table S1.** Site-level RMSE of 106 FLUXNET2015 site for each of the three GPP products considered in this study.

	NIR <sub>v</sub>		BESS		FLUXCOM	
	GPP (Pg C y <sup>-1</sup> )	Fraction (%)	GPP (Pg C y <sup>-1</sup> )	Fraction (%)	GPP (Pg C y <sup>-1</sup> )	Fraction (%)
Evergreen Broadleaf forest	46.74	31.70	40.18	33.66	40.48	34.21
Mixed forest	16.28	11.04	10.61	8.89	11.24	9.50
Woody savannas	15.00	10.17	15.21	12.74	14.12	11.94
Savannas	14.79	10.03	13.08	10.96	13.00	10.99
Croplands	13.82	9.38	10.42	8.73	10.48	8.86
Grasslands	12.11	8.21	9.25	7.75	7.84	6.63
Open shrublands	10.89	7.39	6.01	5.04	6.23	5.27
Cropland/Natural vegetation mosaic	9.74	6.61	8.98	7.52	8.64	7.30
Evergreen Needleleaf forest	4.12	2.80	2.69	2.26	2.87	2.42
Other	1.97	1.34	1.69	1.41	1.55	1.31
Deciduous Broadleaf forest	1.96	1.33	1.24	1.04	1.87	1.58

**Table S2. Per biome distribution GPP for NIR<sub>v</sub>, BESS, and FLUXCOM global GPP products.**

Model Structure	Variance Structure	# fixed params	DIC
GPP intercept + NIR <sub>V</sub> :leaf habit	$a$	4	7142.393
GPP intercept + NIR <sub>V</sub> :leaf habit	$a + b \cdot NIR_V$	4	7134.997
GPP intercept + NIR <sub>V</sub> :leaf habit	$a + e^{zNIR_V} \cdot b$	4	7146.137
GPP intercept + NIR <sub>V</sub> :leaf habit	$a + b \cdot e^{zNIR_V}$	4	7150.204
GPP intercept + NIR <sub>V</sub> :leaf habit	$a + NIR_V^b$	4	7150.299
<b>GPP intercept + NIR<sub>V</sub>:leaf habit</b>	<b><math>NIR_V^b</math></b>	<b>4</b>	<b>7104.392*</b>
GPP intercept + NIR <sub>V</sub> :leaf habit	$a + b * NIR_V^2$	4	7127.383
GPP intercept:leaf habit + slope:leaf habit	$NIR_V^b$	6	7106.333
GPP intercept:land cover + slope:land cover	$NIR_V^b$	22	7106.601
GPP intercept + slope:land cover	$NIR_V^b$	12	7111.44

**Table S3. Potential annual models tested, including various fixed structures and various variance formulations. Variance functions were fit for the standard deviation of both the residual error and the site-level random intercept, where NIR<sub>V</sub> is annual observed NIR<sub>V</sub> for the residual error and the site mean annual NIR<sub>V</sub> for the site random intercept. “zNIR<sub>V</sub>” indicates that NIR<sub>V</sub> values were z-score standardized.**

Site	Latitude	Longitude	Years	Reference
AR-Vir	-28.2395	-56.1886	2009–2012	(10)
AT-Neu	47.1167	11.3175	2002–2012	(11)
AU-ASM	-22.283	133.249	2010–2013	(12)
AU-Ade	-13.0769	131.1178	2007–2009	(13)
AU-Cpr	-34.0021	140.5891	2010–2013	(14)
AU-Cum	-33.6133	150.7225	2012–2013	(14)
AU-DaP	-14.0633	131.3181	2008–2013	(13)
AU-DaS	-14.1593	131.3881	2008–2013	(13)
AU-Dry	-15.2588	132.3706	2008–2013	(13)
AU-Emr	-23.8587	148.4746	2011–2013	(15)
AU-Fog	-12.5452	131.3072	2006–2008	(13)
AU-GWW	-30.1913	120.6541	2013–2014	(16)
AU-RDF	-14.5636	132.4776	2011–2013	(13)
AU-Rig	-36.6499	145.5759	2011–2013	(13)
AU-Tum	-35.6566	148.1517	2001–2013	(17)
AU-Whr	-36.6732	145.0294	2011–2013	(14)
BE-Bra	51.3092	4.5206	2000–2013	(18)
BE-Lon	50.5516	4.7461	2004–2014	(19)
BE-Vie	50.3051	5.9981	2000–2014	(20)
BR-Sa3	-3.018	-54.9714	2000–2004	(21)
CA-NS1	55.8792	-98.4839	2002–2005	(22)
CA-NS2	55.9058	-98.5247	2001–2005	(22)
CA-NS3	55.9117	-98.3822	2001–2005	(22)
CA-NS4	55.9117	-98.3822	2002–2005	(22)
CA-NS5	55.8631	-98.485	2001–2005	(22)
CA-NS6	55.9167	-98.9644	2001–2005	(22)
CA-NS7	56.6358	-99.9483	2002–2005	(22)
CA-Qfo	49.6925	-74.3421	2003–2010	(23)
CH-Cha	47.2102	8.4104	2006–2012	(24)
CH-Fru	47.1158	8.5378	2006–2012	(24)
CH-Oe1	47.2858	7.7319	2002–2008	(25)
CN-Cha	42.4025	128.0958	2003–2005	(26)
CN-Cng	44.5934	123.5092	2007–2010	(27)
CN-Dan	30.4978	91.0664	2004–2005	(28)
CN-Din	23.1733	112.5361	2003–2005	(28)
CN-Du2	42.0467	116.2836	2006–2008	(29)
CN-Ha2	37.6086	101.3269	2003–2005	(30)
CN-HaM	37.37	101.18	2002–2004	(31)
CN-Qia	26.7414	115.0581	2003–2005	(28)
CN-Sw2	41.7902	111.8971	2010–2012	(32)
DE-Akm	53.8662	13.6834	2009–2014	<a href="http://www.fluxdata.org:8080/sitepages/siteInfo.aspx?DE-Akm">http://www.fluxdata.org:8080/sitepages/siteInfo.aspx?DE-Akm</a>
DE-Gri	50.9495	13.5125	2004–2014	(33)
DE-Hai	51.0792	10.453	2000–2012	(34)
DE-Kli	50.8929	13.5225	2004–2014	(35)
DE-Obe	50.7836	13.7196	2008–2014	(36)
DE-RuS	50.8659	6.4472	2011–2014	(37)
DE-Sfn	47.8064	11.3275	2012–2014	(38)
DE-Spw	51.8923	14.0337	2010–2014	<a href="http://www.fluxdata.org:8080/sitepages/siteInfo.aspx?DE-spw">http://www.fluxdata.org:8080/sitepages/siteInfo.aspx?DE-spw</a>
DE-Tha	50.9636	13.5669	2000–2014	(39)
DK-Sor	55.4859	11.6446	2000–2012	(40)
ES-LgS	37.0979	-2.9658	2007–2009	(41)
FI-Hyy	61.8475	24.295	2000–2014	(42)
FR-Gri	48.8442	1.9519	2004–2013	(43)
FR-Fon	48.4764	2.7801	2005–2014	(44)
FR-Pue	43.7414	3.5958	2000–2013	(45)
GF-Guy	5.2788	-52.9249	2004–2012	(46)
IT-BCi	40.5238	14.9574	2004–2014	(47)
IT-CA1	42.3804	12.0266	2011–2013	(48)
IT-CA2	42.3772	12.026	2011–2013	(48)

IT-CA3	42.38	12.0222	2011–2013	(48)
IT-Cp2	41.7043	12.3573	2012–2013	(49)
IT-Isp	45.8126	8.6336	2013–2014	(50)
IT-Lav	45.9562	11.2813	2003–2012	(51)
IT-Noe	40.6061	8.1515	2004–2012	(52)
IT-PT1	45.2009	9.061	2002–2004	(53)
IT-Ren	46.5869	11.4337	2000–2013	(54)
IT-Ro1	42.4081	11.93	2000–2008	(55)
IT-Ro2	42.3903	11.9209	2002–2012	(56)
IT-SR2	43.732	10.291	2013–2014	(57)
IT-SRo	43.7279	10.2844	2000–2012	(57)
IT-Tor	45.8444	7.5781	2008–2013	(58)
JP-MBF	44.3869	142.3186	2003–2005	(59)
JP-SMF	35.2617	137.0788	2002–2006	(59)
NL-Hor	52.2404	5.0713	2004–2011	(60)
NL-Loo	52.1666	5.7436	1996–2013	(61)
RU-Fyo	56.4615	32.9221	2000–2013	(62)
SD-Dem	13.2829	30.4783	2005–2009	(63)
US-AR1	36.4267	-99.42	2009–2012	(64)
US-AR2	36.6358	-99.5975	2009–2012	(64)
US-ARM	36.6058	-97.4888	2003–2012	(65)
US-Blo	38.8953	-120.633	2000–2007	(66)
US-Ha1	42.5378	-72.1715	2000–2012	(67)
US-Los	46.0827	-89.9792	2000–2014	(68)
US-MMS	39.3232	-86.4131	2000–2014	(69)
US-Me2	44.4523	-121.5574	2002–2014	(70)
US-Me6	44.3233	-121.608	2010–2012	(71)
US-Myb	38.0498	-121.765	2011–2014	(72)
US-Ne1	41.1651	-96.4766	2001–2013	(73)
US-Ne2	41.1649	-96.4701	2001–2013	(73)
US-Ne3	41.1797	-96.4397	2001–2013	(73)
US-NR1	40.0329	-105.5464	1998–2014	(74)
US-PFa	45.9459	-90.2723	1995–2014	(75)
US-SRG	31.7894	-110.8277	2008–2014	(76)
US-SRM	31.8214	-110.866	2004–2014	(77)
US-Syv	46.242	-89.3477	2001–2014	(78)
US-Ton	38.4316	-120.966	2001–2014	(79)
US-Twt	38.1087	-121.6530	2009–2014	(80)
US-UMB	45.5598	-84.7138	2000–2014	(81)
US-UMd	45.5625	-84.6975	2007–2014	(82)
US-Var	38.4133	-120.951	2000–2014	(83)
US-WCr	45.8059	-90.0799	2000–2014	(84)
US-Whs	31.7438	-110.052	2007–2014	(77)
US-Wkg	31.7365	-109.942	2004–2014	(85)
ZA-Kru	-25.0197	31.4969	2000–2010	(86)
ZM-Mon	-15.4378	23.2528	2007–2009	(87)

Table S4. The FLUXNET2015 sites used in this study.

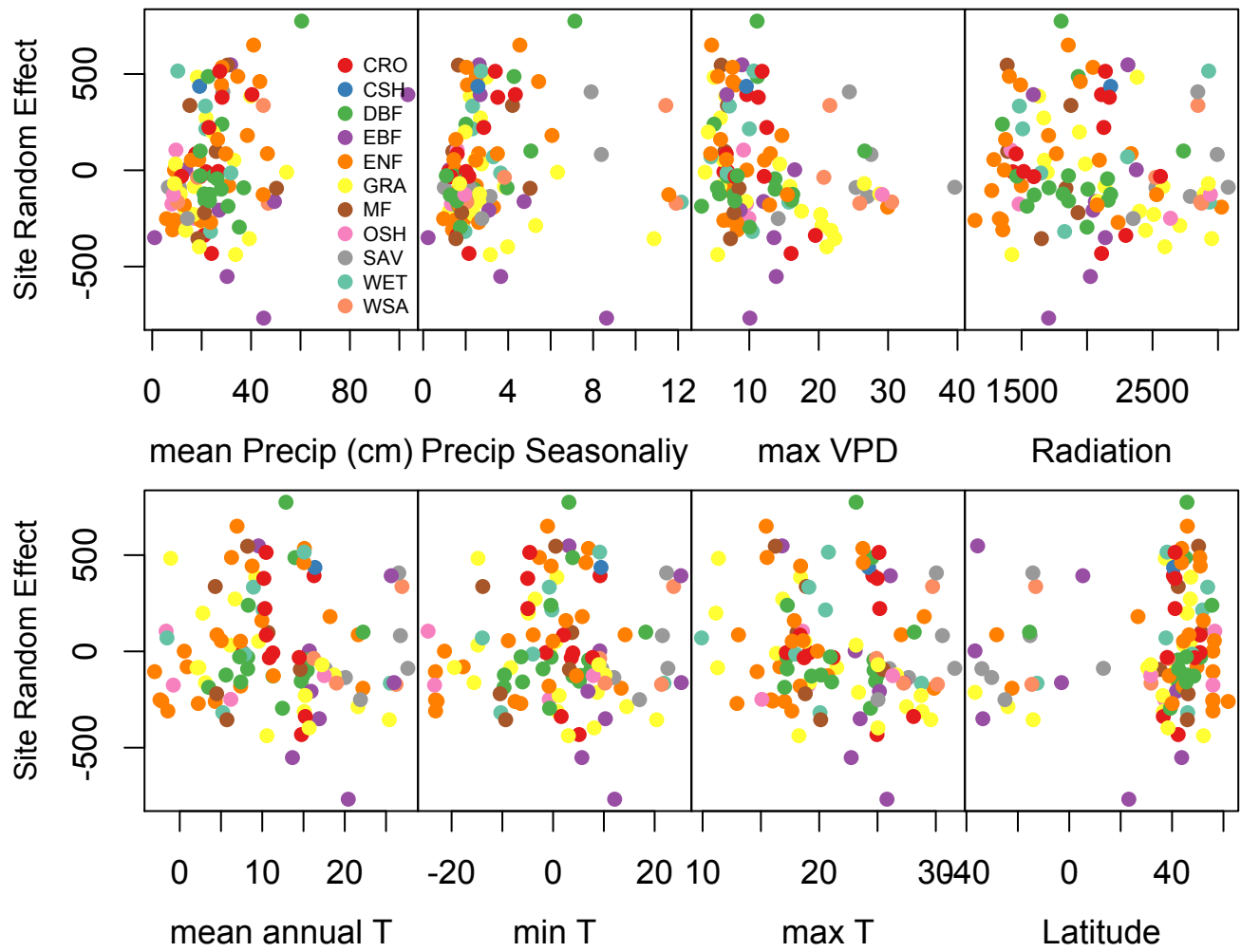


**Fig. S1.** Residuals of the final Bayesian model plotted against various, site-level meteorological data show no coherent patterns, demonstrating that NIR<sub>v</sub> already captures the effects many environmental factors exert on GPP at the annual timescale.

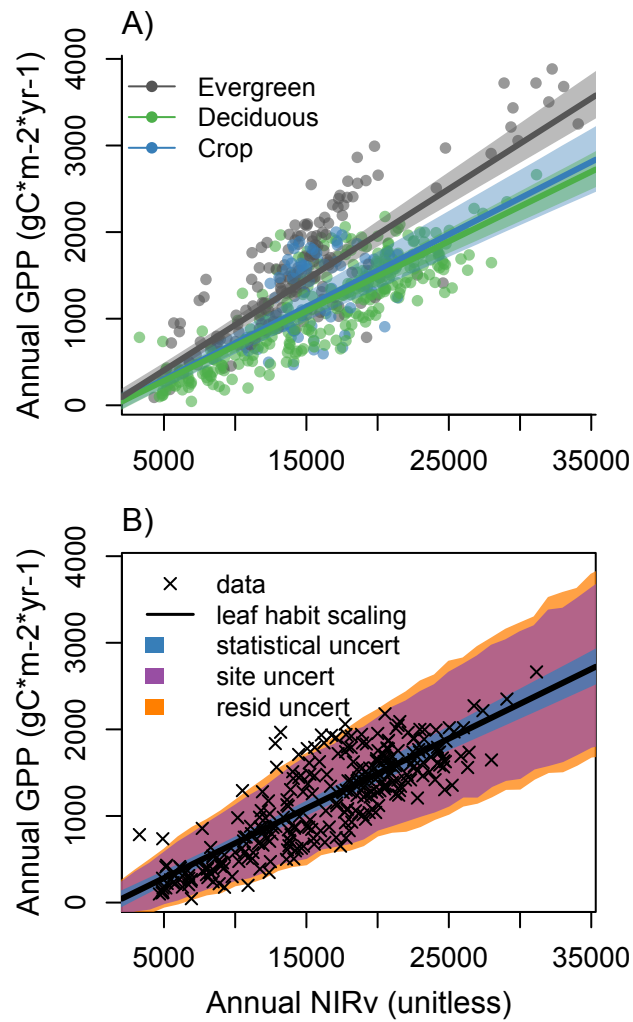


**Fig. S2. Depiction of A) the final model formulation and B) the structure of model uncertainties.** Each leaf habit shared an intercept of 0, but had slightly different NIR<sub>v</sub> to GPP slope. Errors increased exponentially with observed NIR<sub>v</sub>, with site-level uncertainty having the largest relative contribution to total per pixel error.

## 30 References

- 31 1. Hoyer S, Hamman J (2017) xarray: N-D labeled arrays and datasets in Python. *Journal of Open Research Software* 5(1).
- 32 2. McKinney W, et al. (2010) Data structures for statistical computing in python in *Proceedings of the 9th Python in*
- 33 *Science Conference*. (Austin, TX), Vol. 445, pp. 51–56.
- 34 3. Walt Svd, Colbert SC, Varoquaux G (2011) The numpy array: a structure for efficient numerical computation. *Computing*
- 35 *in Science & Engineering* 13(2):22–30.
- 36 4. Hunter JD (2007) Matplotlib: A 2d graphics environment. *Computing in science & engineering* 9(3):90–95.
- 37 5. Waskom M, et al. (2014) seaborn: v0.5.0 (november 2014).
- 38 6. Kluyver T, et al. (2016) Jupyter notebooks – a publishing format for reproducible computational workflows in *Positioning*
- 39 *and Power in Academic Publishing: Players, Agents and Agendas*, eds. Loizides F, Schmidt B. (IOS Press), pp. 87 – 90.
- 40 7. Team RC (2014) R: A language and environment for statistical computing. r foundation for statistical computing, vienna,
- 41 austria. 2013.
- 42 8. Su YS, Yajima M (2015) R2jags: Using r to run ‘jags’. *R package version 0.5-7*.
- 43 9. Plummer M (2013) rjags: Bayesian graphical models using mcmc. *R package version* 3(10).
- 44 10. Posse G, Lewczuk N, Richter K, Cristiano P (2016) Carbon and water vapor balance in a subtropical pine plantation.
- 45 *iForest-Biogeosciences and Forestry* 9(5):736.
- 46 11. Wohlfahrt G, et al. (2008) Seasonal and inter-annual variability of the net ecosystem co2 exchange of a temperate mountain
- 47 grassland: Effects of weather and management. *Journal of Geophysical Research: Atmospheres* 113(D8).
- 48 12. Eamus D, et al. (2013) Carbon and water fluxes in an arid-zone acacia savanna woodland: An analyses of seasonal patterns
- 49 and responses to rainfall events. *Agricultural and Forest Meteorology* 182:225–238.
- 50 13. Beringer J, Hutley LB, Hacker JM, Neininger B, et al. (2011) Patterns and processes of carbon, water and energy cycles
- 51 across northern australian landscapes: From point to region. *Agricultural and Forest Meteorology* 151(11):1409–1416.
- 52 14. Karan M, et al. (2016) The australian supersite network: A continental, long-term terrestrial ecosystem observatory.
- 53 *Science of the Total Environment* 568:1263–1274.
- 54 15. Schroder I (2014) Arcturus emerald ozflux tower site. *OzFlux: Australian and New Zealand Flux Research and Monitoring,*
- 55 *hdl 102(100):14249*.
- 56 16. Prober SM, et al. (2012) Facilitating adaptation of biodiversity to climate change: a conceptual framework applied to the
- 57 world’s largest mediterranean-climate woodland. *Climatic Change* 110(1-2):227–248.
- 58 17. Leuning R, Cleugh HA, Zegelin SJ, Hughes D (2005) Carbon and water fluxes over a temperate eucalyptus forest and a
- 59 tropical wet/dry savanna in australia: measurements and comparison with modis remote sensing estimates. *Agricultural*
- 60 *and Forest Meteorology* 129(3-4):151–173.
- 61 18. Carrara A, et al. (2003) Net ecosystem co2 exchange of mixed forest in belgium over 5 years. *Agricultural and Forest*
- 62 *Meteorology* 119(3-4):209–227.
- 63 19. Moureaux C, Debacq A, Bodson B, Heinesch B, Aubinet M (2006) Annual net ecosystem carbon exchange by a sugar beet
- 64 crop. *Agricultural and Forest Meteorology* 139(1-2):25–39.
- 65 20. Aubinet M, et al. (2001) Long term carbon dioxide exchange above a mixed forest in the belgian ardennes. *Agricultural*
- 66 *and Forest Meteorology* 108(4):293–315.
- 67 21. Miller SD, et al. (2004) Biometric and micrometeorological measurements of tropical forest carbon balance. *Ecological*
- 68 *Applications* 14(sp4):114–126.
- 69 22. Goulden ML, et al. (2006) An eddy covariance mesonet to measure the effect of forest age on land–atmosphere exchange.
- 70 *Global Change Biology* 12(11):2146–2162.
- 71 23. Bergeron O, et al. (2007) Comparison of carbon dioxide fluxes over three boreal black spruce forests in canada. *Global*
- 72 *Change Biology* 13(1):89–107.
- 73 24. Eugster W, Zeeman MJ (2006) Micrometeorological techniques to measure ecosystem-scale greenhouse gas fluxes for
- 74 model validation and improvement in *International Congress Series*. (Elsevier), Vol. 1293, pp. 66–75.
- 75 25. Ammann C, Flechard C, Leifeld J, Neftel A, Fuhrer J (2007) The carbon budget of newly established temperate grassland
- 76 depends on management intensity. *Agriculture, Ecosystems & Environment* 121(1-2):5–20.
- 77 26. Zhang JH, Han SJ, Yu GR (2006) Seasonal variation in carbon dioxide exchange over a 200-year-old chinese broad-leaved
- 78 korean pine mixed forest. *Agricultural and Forest Meteorology* 137(3-4):150–165.
- 79 27. Dong G, et al. (2011) Effects of spring drought on carbon sequestration, evapotranspiration and water use efficiency in the
- 80 songnen meadow steppe in northeast china. *Ecohydrology* 4(2):211–224.
- 81 28. Yu GR, et al. (2006) Overview of chinaflux and evaluation of its eddy covariance measurement. *Agricultural and Forest*
- 82 *Meteorology* 137(3-4):125–137.
- 83 29. Chen S, et al. (2009) Energy balance and partition in inner mongolia steppe ecosystems with different land use types.
- 84 *Agricultural and Forest Meteorology* 149(11):1800–1809.
- 85 30. Fu YL, et al. (2006) Depression of net ecosystem co2 exchange in semi-arid leymus chinensis steppe and alpine shrub.
- 86 *Agricultural and Forest Meteorology* 137(3-4):234–244.
- 87 31. Kato T, et al. (2006) Temperature and biomass influences on interannual changes in co2 exchange in an alpine meadow on
- 88 the qinghai-tibetan plateau. *Global Change Biology* 12(7):1285–1298.
- 89 32. Shao P, Zeng X, Sakaguchi K, Monson RK, Zeng X (2013) Terrestrial carbon cycle: climate relations in eight cmip5 earth
- 90 system models. *Journal of Climate* 26(22):8744–8764.

- 91 33. Gilmanov T, et al. (2007) Partitioning european grassland net ecosystem co<sub>2</sub> exchange into gross primary productivity  
92 and ecosystem respiration using light response function analysis. *Agriculture, ecosystems & environment* 121(1-2):93–120.
- 93 34. Knohl A, Schulze ED, Kolle O, Buchmann N (2003) Large carbon uptake by an unmanaged 250-year-old deciduous forest  
94 in central germany. *Agricultural and Forest Meteorology* 118(3-4):151–167.
- 95 35. Ceschia E, et al. (2010) Management effects on net ecosystem carbon and ghg budgets at european crop sites. *Agriculture,*  
96 *Ecosystems & Environment* 139(3):363–383.
- 97 36. Zimmermann F, Plessow K, Queck R, Bernhofer C, Matschullat J (2006) Atmospheric n-and s-fluxes to a spruce  
98 forest—comparison of inferential modelling and the throughfall method. *Atmospheric Environment* 40(25):4782–4796.
- 99 37. Mauder M, et al. (2013) A strategy for quality and uncertainty assessment of long-term eddy-covariance measurements.  
100 *Agricultural and Forest Meteorology* 169:122–135.
- 101 38. Hommeltenberg J, Schmid HP, Drösler M, Werle P (2014) Can a bog drained for forestry be a stronger carbon sink than a  
102 natural bog forest? *Biogeosciences* 11(13):3477–3493.
- 103 39. Grünwald T, Bernhofer C (2007) A decade of carbon, water and energy flux measurements of an old spruce forest at the  
104 anchor station tharandt. *Tellus B: Chemical and Physical Meteorology* 59(3):387–396.
- 105 40. Pilegaard K, Hummelshøj P, Jensen N, Chen Z (2001) Two years of continuous co<sub>2</sub> eddy-flux measurements over a danish  
106 beech forest. *Agricultural and Forest Meteorology* 107(1):29–41.
- 107 41. Reverter BR, et al. (2010) Analyzing the major drivers of n<sub>2</sub>o in a mediterranean alpine shrubland. *Biogeosciences*  
108 7(9):2601–2611.
- 109 42. Vesala T, et al. (2005) Effect of thinning on surface fluxes in a boreal forest. *Global Biogeochemical Cycles* 19(2).
- 110 43. Loubet B, et al. (2011) Carbon, nitrogen and greenhouse gases budgets over a four years crop rotation in northern france.  
111 *Plant and Soil* 343(1-2):109.
- 112 44. Delpierre N, Berveiller D, Granda E, Dufrene E (2016) Wood phenology, not carbon input, controls the interannual  
113 variability of wood growth in a temperate oak forest. *The New phytologist* 210 2:459–70.
- 114 45. Rambal S, Joffre R, Ourcival J, Cavender-Bares J, Rocheteau A (2004) The growth respiration component in eddy co<sub>2</sub>  
115 flux from a quercus ilex mediterranean forest. *Global Change Biology* 10(9):1460–1469.
- 116 46. Bonal D, et al. (2008) Impact of severe dry season on net ecosystem exchange in the neotropical rainforest of french guiana.  
117 *Global Change Biology* 14(8):1917–1933.
- 118 47. Vitale L, Di Tommasi P, D'Urso G, Magliulo V (2016) The response of ecosystem carbon fluxes to lai and environmental  
119 drivers in a maize crop grown in two contrasting seasons. *International Journal of Biometeorology* 60(3):411–420.
- 120 48. Sabbatini S, et al. (2016) Greenhouse gas balance of cropland conversion to bioenergy poplar short-rotation coppice.  
121 *Biogeosciences* 13(1):95–113.
- 122 49. Fares S, Loreto F (2015) Isoprenoid emissions by the mediterranean vegetation in castelporziano. *Rendiconti Lincei*  
123 26(3):493–498.
- 124 50. Ferréa C, Zenone T, Comolli R, Seufert G (2012) Estimating heterotrophic and autotrophic soil respiration in a semi-natural  
125 forest of lombardy, italy. *Pedobiologia* 55(6):285–294.
- 126 51. Cescatti A, ZORER R (2003) Structural acclimation and radiation regime of silver fir (*abies alba* mill.) shoots along a  
127 light gradient. *Plant, Cell & Environment* 26(3):429–442.
- 128 52. Spano D, Duce P, Snyder RL, Zara P, Ventura A (2005) Assessment of fuel dryness index on mediterranean vegetation in  
129 *Proceedings of the 6th Symposium on Fire and Forest Meteorology, Cammore, Canada.*
- 130 53. Migliavacca M, et al. (2009) Seasonal and interannual patterns of carbon and water fluxes of a poplar plantation under  
131 peculiar eco-climatic conditions. *Agricultural and Forest Meteorology* 149(9):1460–1476.
- 132 54. Marcolla B, et al. (2005) Importance of advection in the atmospheric co<sub>2</sub> exchanges of an alpine forest. *Agricultural and*  
133 *Forest Meteorology* 130(3-4):193–206.
- 134 55. Rey A, et al. (2002) Annual variation in soil respiration and its components in a coppice oak forest in central italy. *Global*  
135 *Change Biology* 8(9):851–866.
- 136 56. Tedeschi V, et al. (2006) Soil respiration in a mediterranean oak forest at different developmental stages after coppicing.  
137 *Global Change Biology* 12(1):110–121.
- 138 57. Matteucci M, Gruening C, Ballarin IG, Seufert G, Cescatti A (2015) Components, drivers and temporal dynamics of  
139 ecosystem respiration in a mediterranean pine forest. *Soil Biology and Biochemistry* 88:224–235.
- 140 58. Galvagno M, et al. (2013) Phenology and carbon dioxide source/sink strength of a subalpine grassland in response to an  
141 exceptionally short snow season. *Environmental Research Letters* 8(2):025008.
- 142 59. Yamazaki T, et al. (2013) A common stomatal parameter set used to simulate the energy and water balance over boreal  
143 and temperate forests. *Journal of the Meteorological Society of Japan. Ser. II* 91(3):273–285.
- 144 60. Van der Molen M, Gash J, Elbers J (2004) Sonic anemometer (co) sine response and flux measurement: Ii. the effect of  
145 introducing an angle of attack dependent calibration. *Agricultural and Forest Meteorology* 122(1-2):95–109.
- 146 61. Dolman A, Moors E, Elbers J (2002) The carbon uptake of a mid latitude pine forest growing on sandy soil. *Agricultural*  
147 *and Forest Meteorology* 111(3):157–170.
- 148 62. Kurbatova J, Li C, Varlagin A, Xiao X, Vygodskaya N (2008) Modeling carbon dynamics in two adjacent spruce forests  
149 with different soil conditions in russia. *Biogeosciences* 5(4):969–980.
- 150 63. Sjöström M, et al. (2009) Evaluation of satellite based indices for gross primary production estimates in a sparse savanna  
151 in the sudan. *Biogeosciences* 6(1):129–138.

- 152 64. Billesbach D, Bradford J (2016) Ameriflux us-ar1 arm usda unl osu woodward switchgrass 1, (AmeriFlux; US Department  
153 of Agriculture; University of Nebraska), Technical report.
- 154 65. Fischer ML, Billesbach DP, Berry JA, Riley WJ, Torn MS (2007) Spatiotemporal variations in growing season exchanges  
155 of co<sub>2</sub>, h<sub>2</sub>o, and sensible heat in agricultural fields of the southern great plains. *Earth Interactions* 11(17):1–21.
- 156 66. Goldstein A, et al. (2000) Effects of climate variability on the carbon dioxide, water, and sensible heat fluxes above a  
157 ponderosa pine plantation in the sierra nevada (ca). *Agricultural and Forest Meteorology* 101(2-3):113–129.
- 158 67. Urbanski S, et al. (2007) Factors controlling co<sub>2</sub> exchange on timescales from hourly to decadal at harvard forest. *Journal*  
159 *of Geophysical Research: Biogeosciences* 112(G2).
- 160 68. Sulman B, Desai A, Cook B, Saliendra N, Mackay D (2009) Contrasting carbon dioxide fluxes between a drying shrub  
161 wetland in northern wisconsin, usa, and nearby forests. *Biogeosciences* 6(6):1115–1126.
- 162 69. Schmid HP, Grimmond CSB, Cropley F, Offerle B, Su HB (2000) Measurements of co<sub>2</sub> and energy fluxes over a mixed  
163 hardwood forest in the mid-western united states. *Agricultural and Forest Meteorology* 103(4):357–374.
- 164 70. Law BE, et al. (2006) *CARBON FLUXES ACROSS REGIONS: OBSERVATIONAL CONSTRAINTS AT MULTIPLE*  
165 *SCALES*, eds. WU J, JONES KB, LI H, LOUCKS OL. (Springer Netherlands, Dordrecht), pp. 167–190.
- 166 71. Ruehr NK, Martin JG, Law BE (2012) Effects of water availability on carbon and water exchange in a young ponderosa  
167 pine forest: Above-and belowground responses. *Agricultural and forest meteorology* 164:136–148.
- 168 72. Sturtevant C, et al. (2016) Identifying scale-emergent, nonlinear, asynchronous processes of wetland methane exchange.  
169 *Journal of Geophysical Research: Biogeosciences* 121(1):188–204.
- 170 73. Verma SB, et al. (2005) Annual carbon dioxide exchange in irrigated and rainfed maize-based agroecosystems. *Agricultural*  
171 *and Forest Meteorology* 131(1-2):77–96.
- 172 74. Monson RK, et al. (2002) Carbon sequestration in a high-elevation, subalpine forest. *Global Change Biology* 8(5):459–478.
- 173 75. Desai AR, et al. (2015) Landscape-level terrestrial methane flux observed from a very tall tower. *Agricultural and Forest*  
174 *Meteorology* 201:61 – 75.
- 175 76. Scott RL, Biederman JA, Hamerlynck EP, Barron-Gafford GA (2015) The carbon balance pivot point of southwestern  
176 u.s. semiarid ecosystems: Insights from the 21st century drought. *Journal of Geophysical Research: Biogeosciences*  
177 120(12):2612–2624.
- 178 77. Scott RL (2010) Using watershed water balance to evaluate the accuracy of eddy covariance evaporation measurements for  
179 three semiarid ecosystems. *Agricultural and Forest Meteorology* 150(2):219–225.
- 180 78. Desai AR, Bolstad PV, Cook BD, Davis KJ, Carey EV (2005) Comparing net ecosystem exchange of carbon dioxide  
181 between an old-growth and mature forest in the upper midwest, usa. *Agricultural and Forest Meteorology* 128(1-2):33–55.
- 182 79. Baldocchi DD, Xu L, Kiang N (2004) How plant functional-type, weather, seasonal drought, and soil physical properties  
183 alter water and energy fluxes of an oak–grass savanna and an annual grassland. *Agricultural and Forest Meteorology*  
184 123(1-2):13–39.
- 185 80. Hatala JA, et al. (2012) Greenhouse gas (co<sub>2</sub>, ch<sub>4</sub>, h<sub>2</sub>o) fluxes from drained and flooded agricultural peatlands in the  
186 sacramento-san joaquin delta. *Agriculture, Ecosystems Environment* 150:1 – 18.
- 187 81. Rothstein DE, Zak DR, Pregitzer KS, Curtis PS (2000) Kinetics of nitrogen uptake by populus tremuloides in relation to  
188 atmospheric co<sub>2</sub> and soil nitrogen availability. *Tree Physiology* 20(4):265–270.
- 189 82. Gough CM, et al. (2013) Sustained carbon uptake and storage following moderate disturbance in a great lakes forest.  
190 *Ecological Applications* 23(5):1202–1215.
- 191 83. Ma S, Baldocchi DD, Xu L, Hehn T (2007) Inter-annual variability in carbon dioxide exchange of an oak/grass savanna  
192 and open grassland in california. *Agricultural and Forest Meteorology* 147(3-4):157–171.
- 193 84. Cook BD, et al. (2004) Carbon exchange and venting anomalies in an upland deciduous forest in northern wisconsin, usa.  
194 *Agricultural and Forest Meteorology* 126(3-4):271–295.
- 195 85. Scott R (2016) Ameriflux us-wkg walnut gulch kendall grasslands, (AmeriFlux; United States Department of Agriculture),  
196 Technical report.
- 197 86. Scholes R, et al. (2001) The environment and vegetation of the flux measurement site near skukuza. *Koedoe* pp. 73–83.
- 198 87. Scanlon T, Albertson J (2004) Canopy scale measurements of co<sub>2</sub> and water vapor exchange along a precipitation gradient  
199 in southern africa. *Global Change Biology* 10(3):329–341.